

Hydrogen pickup during oxidation in aqueous environments: the role of nano-pores and nano-pipes in zirconium oxide films

Jing Hu^a, Junliang Liu^a, Sergio Lozano-Perez^a, Chris Grovenor^a, Mikael Christensen^b, Walter Wolf^b, Erich Wimmer^{b*}, and Erik V. Mader^c

^a Department of Materials, University of Oxford, Parks Road, Oxford, OX1 3PH, UK

^b Materials Design, Inc., 12121 Scripps Summit Drive, San Diego, CA 92131, USA

^c Electric Power Research Institute (EPRI), 3420 Hillview Ave, Palo Alto, CA 94303, USA

*corresponding author, ewimmer@materialsdesign.com, Tel: (760) 495-4924 ext. 301

ABSTRACT

Oxidation of metals by water generates hydrogen which can enter the solid causing serious degradation of its mechanical properties and may also influence the corrosion rate. The present work focuses on hydrogen pickup during the corrosion of zirconium alloys in an aqueous environment. Transmission electron microscopy using Fresnel imaging on three different samples of oxidized Zr has been used to study the type, distribution, concentration and connectivity of nano-porosity as a function of depth through the oxide layer. Extensive interconnected nano-pipes are found in the non-protective outer part of the oxide, while in the protective barrier layer closer to the metal-oxide interface, continuous nano-pipes turn into individual nano-pores. *Ab initio* calculations show that molecular hydrogen is formed spontaneously by the reaction of water with oxygen vacancies in zirconium oxide. Molecular dynamics simulations reveal that these H₂ molecules can diffuse rapidly through nano-pores and nano-pipes as small as 0.5 nm in the oxide layer. Calculations demonstrate that molecular hydrogen dissociates spontaneously on surfaces of suboxides found experimentally at the metal-oxide interface. Oxygen vacancies in ZrO enable the ingress and diffusion of H atoms with an energy barrier of approximately 65 kJ/mol. Further diffusion of hydrogen through oxygen-saturated α -Zr metal is fast, leading to the formation of thermodynamically stable zirconium hydrides. Thus, formation and diffusion of molecular hydrogen through nano-pores in the bulk oxide and ingress of H atoms via suboxides is a possible mechanism of hydrogen pickup in any metal or alloy covered by an oxide scale that contains nano-porosity.

Keywords: *hydrogen pickup; oxide-film constitution; zirconium; transmission electron microscopy; ab initio calculations*

1. Introduction

Corrosion of metals in aqueous environments is seen in almost every aspect of our world where metals and alloys are deployed. Despite the practical importance of this universal process, the exact nature of the underlying mechanisms is still unclear. Dynamic, multi-scale processes lead to the formation of complex, textured oxide films involving metal-oxide and oxide-water interfaces, mass and electron transport, numerous kinds of lattice defects (point defects and grain boundaries), phase transitions, modification of the microstructure by stress, and temperature effects. Alloying elements and second phase particles add further complexity. Thus, trying to understand and simulate all these phenomena on all length and time scales remains a daunting endeavor.

Nevertheless, by combining advanced techniques for nano-scale characterization with state-of-the-art computational approaches, significant progress can be achieved, affording unprecedented insight into some of the critical aspects of this oxidation process.

The chemical reaction of metals with water produces metal oxides and releases hydrogen by a cathodic reaction. This hydrogen either escapes in the form of molecular hydrogen or is picked up by the metal, often leading to degradation of its mechanical strength.

The Zr-water system has a particularly important practical application since Zr alloys are used in light water nuclear reactors as fuel cladding and in fuel assembly components [1]. Hydrogen pickup and the formation of zirconium hydrides is well known to have a detrimental impact on the mechanical properties of these materials [2]. At the high temperatures experienced in loss of coolant accidents (LOCA) zirconium reacts vigorously with water vapor resulting in the rapid production of hydrogen. Mixed with oxygen from air, this can lead to hydrogen explosions as witnessed at the Fukushima power plant in 2011.

There is currently no complete mechanistic understanding of the reaction of water with zirconium, the formation of hydrogen, its transport through the oxide and ingress into the metal despite the large number of publications on this subject. It has been proposed [3-5] that transport of hydrogen through the oxide occurs via solid-state diffusion assisted by oxygen vacancies. Implicitly it is assumed that the diffusing species is H^+ . On the surface of ZrO_2 in contact with water, Sato *et al.* [6] have demonstrated a proton migration mechanism in the form of a cooperative transfer of protons and positive charges involving intermediate water molecules as proton acceptors and donors. Such a mechanism is possible if water is present, which may not be the case close to the Zr metal-oxide interface. In both mechanisms, protons need to enter solid ZrO_2 , which may involve both overcoming an energy barrier and the availability of a sufficiently high concentration of oxygen vacancies or other defects since the solubility of hydrogen in stoichiometric ZrO_2 without oxygen vacancies is extremely low [7]. Cox and Wong pointed out the likely path of hydrogen pickup via structural flaws in the oxide film [8]. Hence, mechanisms involving the hopping of H^+ between -OH groups or the migration of -OH groups along grain boundaries or in cracks are other possibilities [9].

For many years, the detailed structure of the metal/oxide interface has been a subject of interest. In an early study, Iltis and Michel [10] measured a thin layer of a sub-oxide without suggesting a clear composition. More recent studies have been able to show that this sub-oxide has a stoichiometry close to ZrO . For instance, analysis of Zircaloy-2 samples oxidized in a steam autoclave [11] revealed a sub-oxide with an oxygen content of approximately 50 at. % and a layer thickness of about 200 nm. Similar studies on other commercial alloys corroded in pressurized water showed varying thicknesses of the same metastable ZrO suboxide at different stages of the oxidation process [12-15]. All these authors also observed an oxygen concentration gradient over a distance of 200 - 400 nm into the metal from a level close to the sub-oxide of about 30 at. % down to a few atomic percent. In addition, several different types of nano-porosity have been observed in the oxide close to the metal/oxide interface by Fresnel imaging in a transmission electron microscope [16]. Recent positron annihilation Doppler broadening spectroscopy experiments on oxides on Zircaloy-4 samples have also identified a heavy supersaturation of

oxygen vacancy complexes near the metal oxide interface that the authors suggest could develop into these nano-scale pores [17].

There has been a good deal of focus on the concept that H transport through the oxide occurs preferentially along grain boundaries. Extensive computational studies by Panas and coworkers [18,19 and references therein] have provided detailed insight into the role of oxygen vacancies and alloying elements at grain boundaries in the oxidation of zirconium. Recently, these authors have demonstrated evidence for the possible alignment of oxygen vacancies in tetragonal ZrO_2 , causing a “nano-pore mediated HPU-avalanche”. Thus, both grain boundaries and local porosity can offer pathways for hydrogen ingress to the metal matrix, and which are activated depends on the environmental conditions.

In this paper we focus on the formation, transport, and pickup of hydrogen for the system water/ α -zirconium, demonstrating the possible role of molecular hydrogen in this process. While small amounts (typically less than 2%) of alloying elements such as Fe, Ni, Cr, Sn, and Nb play an important role in zirconium alloys, the overall mechanism described in the present work is of generic nature and independent of a specific zirconium alloy, although we are well aware that these alloying elements effect the rates of this process [20,21]. The mechanism for hydrogen transport described here could also be relevant for any metal or alloy which forms a nano-porous oxide scale.

2. Experimental Methods

Three materials were used in the experimental part of this work; model Zr-0.5Nb and Zr-1Nb alloys and commercial Zircaloy-4, all supplied by the Westinghouse Electric Company in the recrystallized (RXA) condition. Small samples were oxidized in an autoclave in pure water at 360 °C and 18 MPa. The choice of these samples was to explore whether the distribution of nanoscale porosity was the same in oxides grown on different Zr alloys and at different stages of the oxidation process. The Zr-0.5Nb and the Zircaloy-4 samples were taken at a relatively early stage of aqueous corrosion, before the first kinetic transition, while the Zr-1Nb sample is taken well past this first transition. The values for hydrogen pick-up fraction (HPUF) in the metal matrix for these samples were also measured. Detailed sample information and corrosion data are summarized in Table 1 and Figure 1.

Table 1
Summary of sample information and corrosion data.

Sample ID	Composition (wt%)	Corrosion time (days)	Weight gain (mg/dm ²)	Hydrogen (ppm)	Avg. oxide thickness (nm)	HPUF
Zr-1Nb	Zr-1.03Nb-0.05Fe	225	61.8	106	4.0	12%
Zr-0.5Nb	Zr-0.53Nb-0.04Fe	75	31.4	5	2.1	1%
Zircaloy-4	Zr-1.36Sn-0.21Fe-0.11Cr	60	26.1	7	1.7	3%

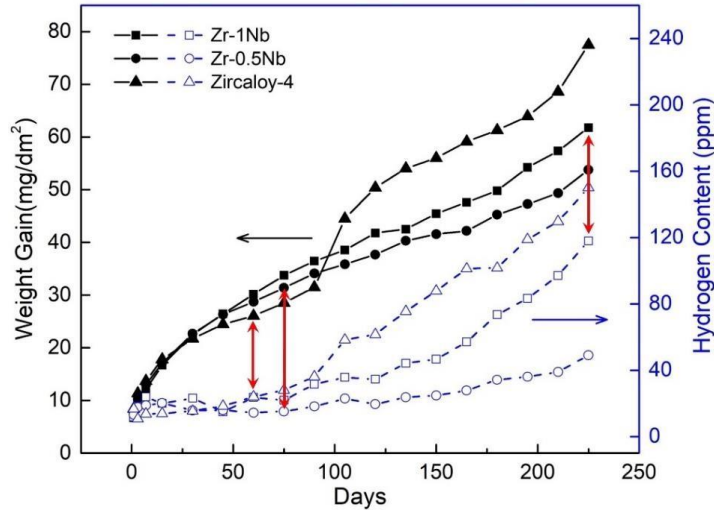


Fig. 1. Weight gain and hydrogen pickup curves for the three selected corroded Zr-alloy materials. The specific samples selected for study are highlighted by the red arrows.

Cross sectional transmission electron microscopy (TEM) foils containing both the oxide layer and the metal matrix were prepared using the in-situ lift-out FIB method [22] with an initial milling current of 7000 pA, gradually decreasing to 300 pA at 30 kV, and further thinned to a uniform thickness of ~ 50 nm using a low energy beam at 2 kV and 200 pA. This is very important to avoid the complex images that result with specimens much thicker than the oxide grain size. There will of course be some stress relaxation during FIB-extraction process to make these very thin TEM specimens, but the primary use of TEM in this work is in detecting systematic differences in the distribution and concentration of buried nano-porosity from samples at selected stages of the oxidation process. All the TEM specimens have been prepared using the same FIB-techniques, so any differences in the characteristic porosity observed between the samples are unlikely to be a result of the sample preparation technique [12,15]. TEM characterization of the distribution of pores was carried out using a JEOL 2100 LaB₆ microscope operated at 200 kV. The morphology of nano-pores can be revealed clearly using Fresnel imaging conditions [23,24]. Under these conditions, buried pores show dark contrast in over-focused conditions and bright contrast in under-focused conditions. Since the images depend strongly on the selected defocus value (Δf), here $\Delta f = \pm 1000$ nm was used for consistency for all the results shown. In order to determine the distribution of pores through the thickness of the oxide, a series of Fresnel images were captured at various distances from the metal-oxide (O/M) interface in each sample. For the first time, we have also carried out a quantitative analysis of nano-porosity concentration as function of oxide depth in the Zr-0.5Nb sample. Because the nano-pores (typically 2 – 5 nm in diameter) are distributed in a 3-dimensional array in the TEM thin foil, the apparent number density will change with sample thickness, and thus a precise local thickness measurement is required. The thicknesses of the regions of interest were determined to be 40-60 nm using Electron Energy Loss Spectroscopy (EELS) in a JEOL ARM 200F microscope

operating at 200 kV with a step size of 10 nm, a convergence angle of 30 mrad and a collection angle of 40 mrad using the method described in [25].

A quantitative measurement of the concentration of nano-pores and nano-pipes as a function of location in the oxide was performed for the Zr-0.5Nb sample. To improve the statistical significance, three large regions (~500 nm by 500 nm) were selected at different oxide depths, and at least three high-magnification micrographs were taken from each of these regions. The concentration of nano-porosity was then defined as the total length of nano-pores and nano-pipes along the corrosion direction per unit sample volume.

3. Computational Methods

The structure and energy of zirconium oxides, their surfaces, and their interactions with water and hydrogen were computed using density functional theory (DFT) [26,27] with the generalized gradient approximation describing electronic exchange-correlation effects as given by Perdew *et al.* [28]. The resulting effective Schrödinger equations were solved using the projector augmented wave method [29] as implemented in the Vienna ab-initio simulation package (VASP) [30,31] within the MedeA[®] materials modelling platform [32]. Energy barriers for processes such as the ingress of H into suboxide and diffusion barriers inside suboxide were determined either by a drag method or by the nudged elastic band method [33]. In the drag method, an H atom is moved stepwise in one direction, for example perpendicular to a surface, and the total energy is minimized in each step by allowing the moving atom to relax in the two directions perpendicular to the drag direction and all other atoms to relax without constraints. This method is well suited to investigate energy barriers for the ingress of H from a surface into the interior of a solid. The nudged elastic band method finds the lowest energy path between an initial and a final configuration by constrained minimization of the energy and forces for a series of intermediate configurations connecting the initial and final state.

Processes such as the diffusion of water and hydrogen molecules in nano-pipes without bond-breaking were simulated by molecular dynamics using a valence forcefield, *i.e.* a description of interatomic interactions for systems with predefined interatomic bonds such as Zr-O or O-H bonds and so-called non-bonding interactions, namely long-range electrostatic interactions, weak van der Waals attractions and short-range repulsion, for example between hydrogen and water molecules. In the present work, the functional form for such a valence forcefield is that given by Sun *et al.* [34]. The parameters optimized for the present zirconium oxide are listed in Table 2 employing the Waldman-Hagler combining rules [35] for the van der Waals interactions. The parameters for water and molecular hydrogen were taken from the pcff+ forcefield as implemented in the MedeA[®] software [32].

The development of additional parameters needed to describe the structure and flexibility of ZrO₂ were guided by experimental crystallographic data and *ab initio* calculations. The resulting forcefield for t-ZrO₂ reproduces well the experimental density, lattice parameter and interatomic

distances of this oxide. At elevated temperature, as used in the present application, molecular dynamics simulations show some flexibility of the lattice while maintaining its overall structure including nano-pores and nano-crevices. This is sufficient for the present purpose. Any other use of this forcefield for t-ZrO₂ beyond the current scope would require additional parameter optimization or a different type of interatomic potential. However, the important interactions between the water molecules, the dissolved H₂ molecules and the hydroxylated oxide surfaces are well described by the present forcefield. The molecular dynamics simulations have been carried out with the Large-scale Atomic/Molecular Massively Parallel Simulator (LAMMPS) [36] as integrated in the MedeA[®] platform.

Table 2

Forcefield parameters for the molecular dynamics simulations of water interacting with hydroxylated surfaces of tetragonal ZrO₂.

Forcefield term		Parameters (energies in units based on kcal/mol)					
		b ₀ (Å)	k ₂	k ₃	k ₄		
<i>Bond stretching</i>							
<i>E^b</i> (Zr-O), O inside oxide		2.135	1000	0		0	
<i>E^b</i> (Zr-O), O of -Zr-OH group		2.2	1000	0		0	
<i>E^b</i> (H-O), H of -Zr-OH group		0.97	700	-1500		1800	
<i>E^b</i> (H-O), H of H ₂ O		0.97	563.28	-1428.905		2004.7658	
<i>E^b</i> (H-H), H of H ₂		0.7412	414.2185	-805.6549		914.1296	
<i>Bond angles</i>		<i>θ₀</i> (deg)					
<i>E^a</i> (O-Zr-O)		112.3	-300	0		0	
<i>E^a</i> (Zr-O-H)		112.3	-300	0		0	
<i>E^a</i> (Zr-O-Zr)		120.3	-300	0		0	
<i>E^a</i> (H-O-H) in water		103.7	49.84	-11.6		-8.0	
	Zr	O in Zr	O in-ZrOH	H in-ZrOH	O in water	H in water	H in H ₂
<i>Charges</i>	1.6	-0.8	-0.8	0.4	-0.806	0.403	0
<i>Non-bond r⁰</i>	3.5	3.38	3.5	1.05	3.608	1.098	1.421
<i>Non-bond ε</i>	0.1	0.1	0.07	0.08	0.274	0.013	0.0216

4. Results

4.1 Experimental observations on the morphology of nano-pores and nano-pipes in ZrO₂ and at the metal-oxide interface

Previous work on the microstructure of oxide films on zirconium fuel cladding alloys has been carried out using X-ray diffraction [37,38], scanning electron microscopy (SEM) [37,39,40],

conventional TEM [12,41-45], transmission Kikuchi diffraction [14,15] and crystal orientation mapping in the transmission electron microscopy mode, giving a clear picture of the characteristic features. The bulk oxide is predominantly monoclinic with some stress-stabilized tetragonal oxide near the metal-oxide interface. Generally, the outer 100-700 nm of the oxide contains small equiaxed grains, 20–30 nm in diameter, and under this equiaxed layer there are layers of larger elongated columnar grains oriented parallel to the oxide growth direction. The thin layer of ZrO sub-oxide described above is often found at the metal/oxide interface in materials from both of the major classes of zirconium fuel cladding alloys (Nb-containing and Nb-free) [12-15]. Thus from the water-ZrO₂ surface, any in-diffusing species will encounter bulk polycrystalline ZrO₂, possibly a thin ZrO suboxide layer and oxygen-saturated Zr metal – Zr(O_{sat}) (~ 30 at% O) [12,14,15,24] before reaching the underlying bulk metal. For the three samples in this study, we used EELS multiple linear least squares (MLLS) phase mapping to identify the ZrO and Zr(O_{sat}) phases. It is found that the 225-day Zr-1Nb sample has ZrO suboxide grains forming a sawtooth layer of around 130 nm thickness, followed by a uniform 180 nm Zr(O_{sat}) layer. The Zr-0.5Nb and Zircaloy-4 samples have thinner suboxide layers, around 100 nm, plus a 100 nm Zr(O_{sat}) layer. It is within these variations in local microstructure that we have now analyzed the morphology and distribution of nano-porosity, and systematic differences were observed at different locations in the oxides.

As an example of this kind of analysis, the set of high-resolution over-focused images in Figure 2(a) show the types of nano-pores observed as a function of depth through a typical oxide layer grown on the Zr-1.0Nb sample corroded for 225-days. Close to the metal-oxide interface, where we expect the oxide to be electrochemically protective, the so-called barrier layer [46-48], several different kinds of nanoscale porosity can be seen. Around 200 nm from the interface, some of the grain boundaries between the columnar oxide grains are decorated with a ‘string-of-pearls’ arrangement of interconnected porosity that we have termed *nano-pipes* (a-3). The individual pores become gradually less well connected closer to the metal/oxide interface (a-2, a-3), so that <200 nm from the interface mostly isolated 1-3 nm pores are observed within the oxide grains (a-2), although there is a rare example of a nano-pipe running right down to the oxide/sub-oxide interface in a-1. At the same location, we can identify flake-shaped porosity/nano-cracking 5-10 nm in length running parallel to the metal-oxide interface (a-2). At the end of some of the columnar ZrO₂ grains in (a-1) there is also continuous porosity at the zirconia-suboxide interface. Individual pores are also observed in the ZrO suboxide layer (a-1). This kind of complex, partly interconnected porosity has been suggested to play an important role in the rate-determining oxygen transport processes during corrosion [12,49]. In the present context, nano-porosity near the oxide-metal interface could provide pathways for the diffusion of molecular hydrogen, as will be discussed below.

Further from the metal-oxide interface, more continuous interconnected nano-pores/nano-pipes are observed along many of the grain boundaries, and some of these have evolved into larger micro-cracks (a-4). From this observation, we suggest that the outer layers of oxide are short circuited in the overall electrochemical corrosion cell, so that the only protective barrier layer will be the thin oxide layer between the nearest interconnected nano-pipes and the underlying metal. This is consistent with in-situ electrical impedance spectroscopy measurements taken at multiple points through the pre-transition period, where the impedance characteristics of the developing corrosion

film is found to take on the characteristics of an outer "porous" layer and an inner "protective" layer [50].

Figures 2 (b) and (c) show the results of the same through-depth porosity analysis for Zr-0.5Nb and Zircaloy-4 samples, respectively. The two Zr-Nb alloy samples have similar oxide nanostructures even though they are at different stages in the corrosion process. If we define the barrier layer as the region where only isolated pores can be identified, both of these two alloys have a similar barrier thickness of ~200 nm (b-1, b-2, b-3). Above that layer, a porous structure with continuous interconnected nano-pores/pipes is observed, (b-4). The Zircaloy-4 alloy has a similar corrosion rate to the 0.5Nb alloy [51] but with a hydrogen pick up fraction (HPUF) at least 3 times higher for the samples studied (Table 1). The results in Figure 2(c) show that the apparent barrier layer in the oxide on Zircaloy-4 (the region free of interconnected porosity) is only ~100 nm thick (c-1, c-2), and more continuous nano-pipes and nano-cracks can be found throughout the porous oxide (c-3, c-4). In comparison, as mentioned above, the two Zr-Nb alloys have barrier thickness of ~200 nm. This may be a result of the higher volume fraction of equiaxed grains seen in oxides on the Zircaloy-4 sample [39,52], and suggests an easy transport path for hydrogenic species that can explain the higher measured HPUF value for this material.

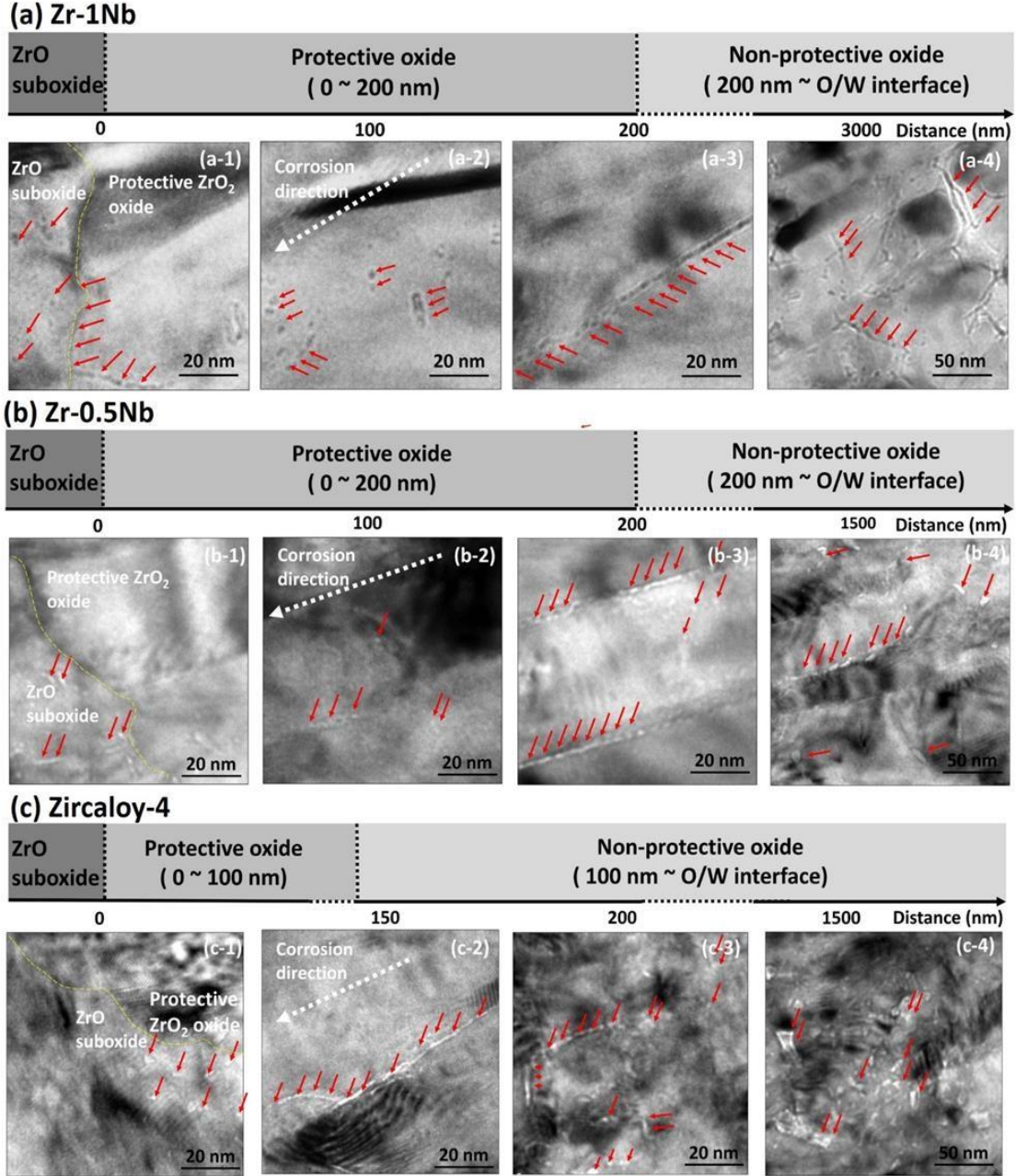


Fig. 2. Nano-porosity as function of depth in the oxide on three Zr alloys: (a) Zr-1.0Nb 225-day, (b) Zr-0.5Nb 75-day, (c) Zircaloy-4 61-day. TEM Fresnel images from samples ($\Delta f = \pm 1000$ nm so the porosity shows dark/white contrast) showing the distribution of nano-porosity as function of depth through the oxide. Nano-pores/pipes are highlighted by red arrows and the ZrO_2/ZrO interface is highlighted by the yellow dashed line in (a-1, b-1, c-1). Protective and non-protective oxide is marked on top of the images.

4.2 Simulations of the ingress of water into nano-pores and nano-pipes and reactions with ZrO_2

In the presence of nano-pipes and nano-pores in the oxide film as shown in the previous section, water molecules from the aqueous phase can readily diffuse through the oxide film. The

experiments presented above resolve nano-pipes and nano-pores of the size of several nanometers, and the present simulations reveal that water molecules (with diameter on the order of 0.3 nm) can diffuse in nano-pipes with a diameter as small as about 1 nm while hydrogen molecules can diffuse through nano-pipes as long as the nano-pipe diameter is larger than about 0.5 nm, as illustrated in Figure 3. Here, ZrO_2 is represented by the tetragonal phase mostly for computational convenience. In the present consideration of the diffusion of water and hydrogen molecules in nano-pipes, the key aspect is the spacing between the walls of the nano-cracks and nano-pores and their coverage with hydroxyl groups rather than the details of the interior of the solid phase. It should be noted, though, that prior to sample preparation, t- ZrO_2 may exist at the metal-oxide interface as this phase is stress-stabilized.

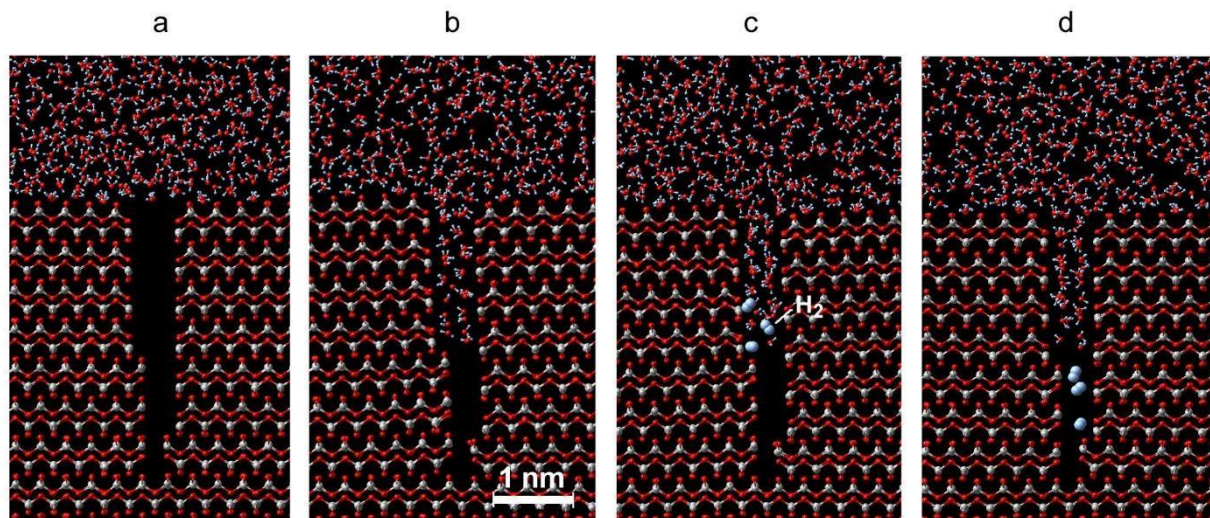


Fig. 3. Ingress of water molecules into pores of ZrO_2 and H_2 diffusion. The c -axis of t- ZrO_2 is perpendicular to the water/oxide interface; the side-walls of the crack are (100) planes; (a) model of a nanopore in t- ZrO_2 with water at 550 K and 150 bar; (b) ingress of water into the pore after 50 ps of molecular dynamics; (c) generation of molecular hydrogen by reaction of water with vacancies in side walls; (d) diffusion of H_2 molecules into the pore of about 0.5 nm width. For clarity, the hydrogen atoms in the H_2 molecules are visualized as large, light-blue spheres. Note that H_2 molecules diffuse through pores which are too narrow for water, thus reaching closer to the metal/oxide interface.

Two different cases of reactions of water molecules with oxide surfaces are considered here. The first case involves stoichiometric surfaces and the second case sub-stoichiometric surfaces. Water molecules can react with stoichiometric surfaces of ZrO_2 , as they may exist at the oxide/water interface and on the walls of pores. Quantum mechanical simulations reveal spontaneous dissociation and formation of surface hydroxides. This process is common for many metal oxides reacting with water [53-55]. If this reaction involves the breaking of Zr-O bonds at the surface, and if reactive species such as $\text{O}_2^{\cdot-}$ are present, *e.g.* from radiolysis, Zr ions can be dissolved leading to initiation of cracks, as discussed by Cox [56].

A quite different process occurs when water molecules reach oxygen vacancy sites, as they are likely to be present in regions close to the metal-oxide interface. *Ab initio* simulations of the reaction of water with sub-stoichiometric oxide surfaces reveal a strongly exothermic dissociation of water molecules. When a water molecule reacts with an oxygen vacancy, the site is filled with the oxygen atom from the water molecule and two hydrogen atoms are released, which bind in two neighboring sites as shown in Figure 4.

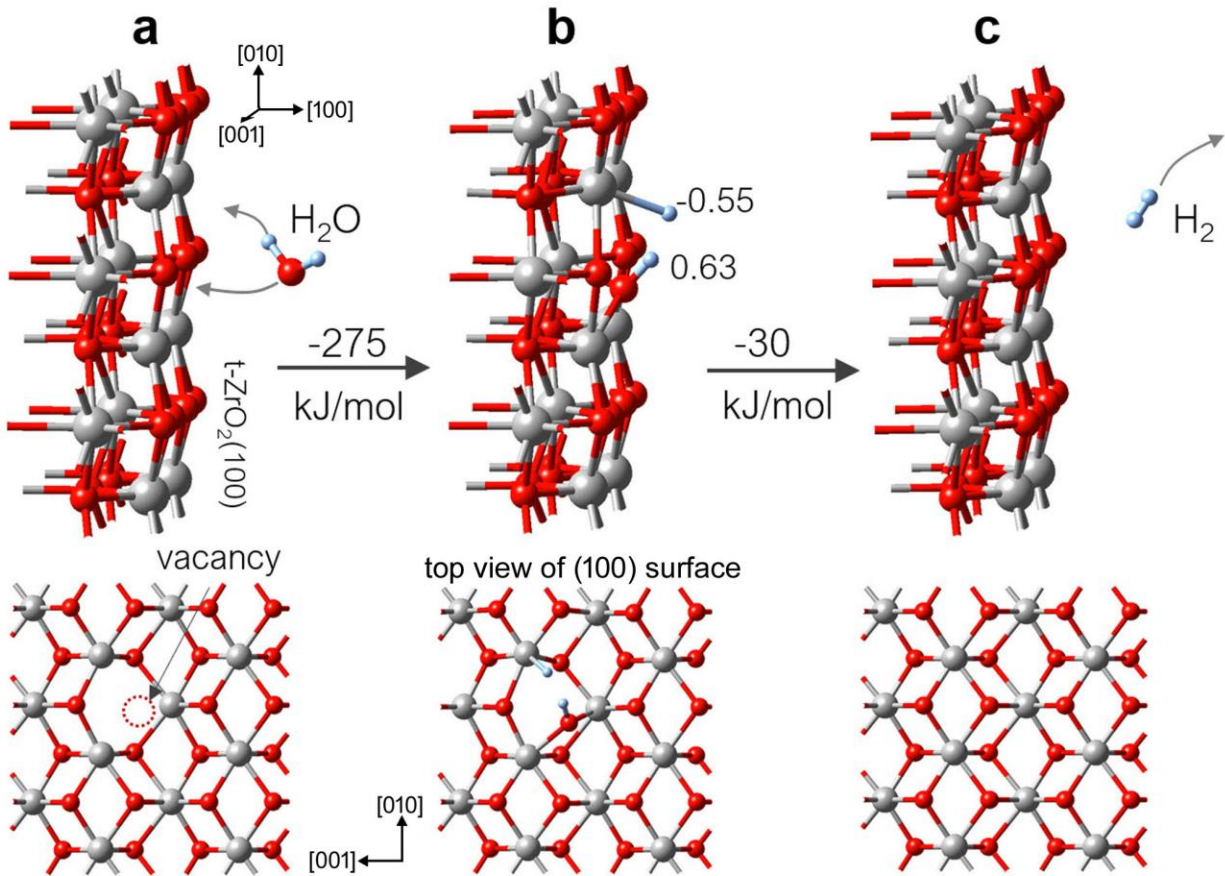


Fig. 4. Reaction of a water molecule with an oxygen vacancy on a t-ZrO₂(100) surface. (a) a water molecule approaches an oxygen vacancy on a t-ZrO₂(100) surface; (b) with a release of 275 kJ/mol the water molecule is chemisorbed and dissociated. The oxygen atom fills the vacancy, one H atom remains attached to O, the other H atom binds to Zr; the values next to the H atoms are atomic charges; (c) formation and desorption of H₂ molecule with a significant exothermic reaction enthalpy. The structures and energies are obtained from *ab initio* calculations. The ZrO₂ surface is represented by a slab and only the top layers are shown for clarity.

One of the H atoms of the water molecule remains attached to the oxygen atom that fills the vacancy whereas the other H atom binds to a Zr atom. The charges of these two H atoms have opposite sign, as obtained from quantum mechanical calculations employing the so-called Bader charge analysis [57]. The H atom attached to O has a positive charge (0.63), and thus could be termed “acidic H” while the H atom bonded to Zr has a negative charge (-0.55), *i.e.* it can be called “hydridic H”. These two H atoms can recombine and escape as H₂ molecule in an exothermic

reaction. With increasing temperature, entropy favors the formation of H_2 molecules, thus this reaction is likely to occur. It is important to note that this reaction requires the initial oxygen vacancy to be neutral, *i.e.* the energy levels corresponding to the dangling bonds of the Zr atoms adjacent to the vacancy are occupied. Using an Ellingham diagram for the reaction $Zr + \frac{1}{2}O_2 \rightarrow ZrO_2$, the partial pressure of O_2 at the metal/oxide interface is of the order of 10^{-90} atm. From a Brouwer diagram, at 360 °C (633 K) the concentration of neutral oxygen vacancies is higher than that of positively charged vacancies below an oxygen partial pressure of approximately 10^{-70} atm. This implies that neutral oxygen vacancies are likely to exist in the proximity of the metal/oxide interface. Another way of rationalizing this scenario comes from an analysis of the electronic band structure. The electronic level associated with the oxygen vacancy is in the band gap of ZrO_2 approximately 2 eV below the minimum of the conduction band. Hence, if electrons occupy the bottom of the conduction band, they can neutralize the oxygen vacancy states. Of course, there will be some differences between m- ZrO_2 , t- ZrO_2 , and hexagonal ZrO .

In the case of a positively charged surface vacancy, as may exist near the water/oxide interface, the adsorption and dissociation of a water molecule filling the vacancy is still strongly exothermic, but both H atoms remain bonded to surface oxygen atoms. In this case, the formation of molecular hydrogen requires supply of additional electrons for a cathodic reaction to occur. This aspect of the corrosion process involves the transport of oxygen ions and charge transport, which is highly complex and beyond the scope of the present paper focusing on H transport.

The (100) surface of t- ZrO_2 is one of many possible reactive surfaces, but it is reasonable to assume that other surfaces containing O vacancies exhibit similar properties. For example, computations performed for the t- ZrO_2 (001) surface show the same overall reaction pattern, albeit with somewhat different specific values for the reaction enthalpy. Hence, it is reasonable to assume that this reaction mechanism applies to a range of different surfaces whenever an oxygen vacancy is present, including surfaces of monoclinic ZrO_2 which is the more likely structure in oxides formed by aqueous corrosion [52,58-60].

After the dissociation of a water molecule by filling a neutral vacancy in ZrO_2 in a crack or nano-pore, one could imagine that the hydrogen atoms enter the bulk oxide and diffuse within the oxide. However, computations of H atoms migrating from the oxide surface into bulk ZrO_2 demonstrate that this process is unlikely due to high energy barriers for H ingress into oxides [61]. Thus, it is reasonable to assume that H_2 molecules are produced as a result of water molecules reacting with oxygen vacancies on inner surfaces of the oxide layer.

While transport of hydrogen in the form of protons along hydroxylated grain boundaries is very likely to occur, for example via a Grotthuss mechanism as investigated by Sato *et al.* [6] and possibly also in “dry” grain boundaries containing hydroxyl groups, transport in this form involves energy barriers that can be significant. In contrast, transport of hydrogen in molecular form is essentially without barriers and thus very fast, provided that channels of sufficient width are present, as described in the present work.

4.3 Diffusion of H_2 molecules in nano-pores and nano-pipes and reaction with suboxide and oxygen-saturated Zr

If H_2 molecules are formed close to the oxide/water interface, they are likely to escape into the aqueous phase. If, on the other hand, the above reaction takes place deeper inside the oxide film and if there is a network of nano-pores reaching the region of suboxide or the metal-oxide interface, H_2 molecules can diffuse in these nano-pores if the diameter is at least 0.5 nm. This is the result of molecular dynamics simulations using a classical forcefield as illustrated in panel (d) of Figure 3.

As evident from the experimental characterization of oxide films on similar samples, a zirconium suboxide (ZrO) is often found, and oxygen-saturated α -Zr metal (Zr_3O) is always observed in the interface region between the metal and the zirconium dioxides [13-15,62]. In the following it will be demonstrated that these suboxides can play a critical role in the dissociation and pickup of hydrogen.

Computations reveal that on surfaces of ZrO , Zr_3O , and Zr , molecular hydrogen can dissociate spontaneously releasing a significant amount of heat. As illustrated in Figure 5 for a Zr_3O (0001) surface, the dissociation of an H_2 molecule on this surface releases 94 kJ/mol per H atom.

For the resulting chemisorbed H atoms on the $Zr_3O(0001)$ surface, DFT calculations reveal an equilibrium position in three-fold hollow sites. These H atoms are slightly negatively charged, *i.e.* they are hydridic in nature. In fact, the equilibrium position of H in pure α -Zr as well as in hydrides are tetrahedral sites with similar bond lengths as H chemisorbed on the $Zr_3O(0001)$ surfaces in three-fold hollow sites. Similar processes occur on other crystallographic surfaces of Zr_3O as well as on ZrO and on pure Zr . It is worthwhile noting that O-saturated Zr metal contains up to about 30% oxygen. In this case, about 1/3 of all octahedral interstitial sites of the hexagonal close-packed lattice of α -Zr are occupied with interstitial oxygen atoms, either disordered or ordered. Thus, the Zr_3O structure shown Figure 5 also represents O-saturated Zr metal.

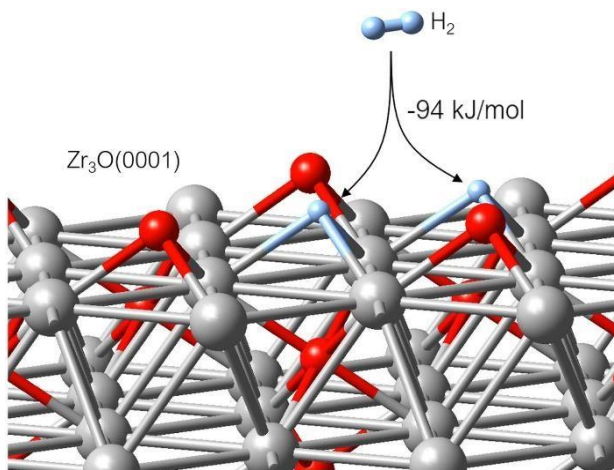


Fig. 5. Dissociation of an H_2 molecule on a $Zr_3O(0001)$ surface. The reaction releases 94 kJ/mol per H atom. Computations reveal an equilibrium position of H atoms occupying three-fold hollow sites on this surface.

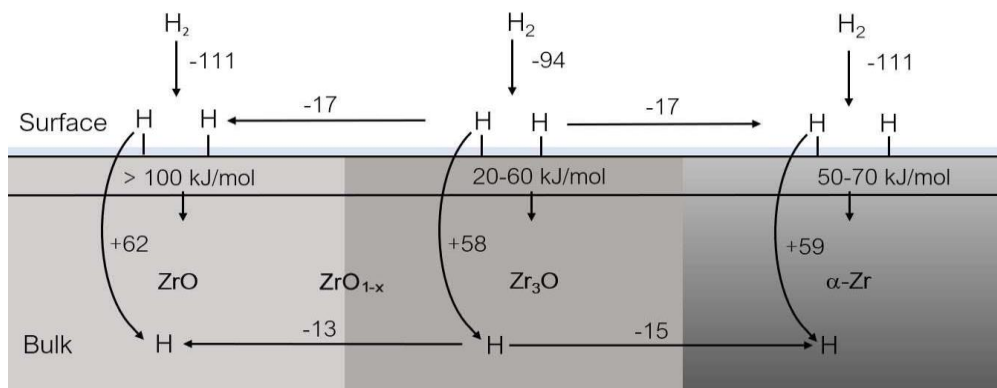


Fig. 6. Energies of dissociation of H_2 and barriers for ingress into Zr and its suboxides. The dissociation of molecular hydrogen and the chemisorption on the surfaces of ZrO , Zr_3O , and Zr are strongly exothermic, namely -111, -94, and -111 kJ/mol, respectively. The barrier for ingress of H atoms is lowest for Zr_3O and highest for ZrO , as shown in the row below the surface. At low H coverage, the transfer of H from the surface into the bulk requires an energy between 58 and 62 kJ/mol. Increasing H coverage will raise the chemical potential of adsorbed H, thus facilitating the ingress.

The next step in the hydrogen pickup process is the ingress of H atoms from the suboxide surfaces into the interior of these phases. The present computations demonstrate that this could be a rate-limiting step, especially if there is a layer of dense zirconium monoxide. However, the oxygen-saturated Zr (Zr_3O) exhibits a barrier for the ingress of H as low as 20 kJ/mol. A summary of the barriers for H pickup into ZrO , Zr_3O , and Zr is illustrated in Figure 6.

In all cases shown in Figure 6, H atoms are more stable on surfaces than in the bulk. However, this holds only for isolated H atoms on the surfaces of Zr metal, oxygen-saturated $Zr(O_{sat})$, Zr_3O , and ZrO -suboxide phases. As the coverage increases, the chemical potential of H atoms chemisorbed on these surfaces rises. Together with entropic effects, at a certain concentration it becomes favorable in terms of Gibbs free energy for H to migrate into the bulk phase rather than remaining as chemisorbed species.

In fact, it is reasonable to assume that the “surfaces” underlying Figures 5 and 6 are in reality nano-scale patches of suboxide adjacent to nano-pores, where the relative H concentration could be quite high, thus providing a thermodynamic driving force to overcome the barriers for H ingress and to spread inside the bulk phases.

The present calculations show that fully stoichiometric hexagonal ZrO presents a high barrier for H ingress whereas the presence of oxygen vacancies in the ZrO phase greatly reduces this barrier. In fact, calculations of the diffusion barrier of H atoms give a value of above 200 kJ/mol in fully stoichiometric hexagonal ZrO while the presence of oxygen vacancies reduces the barrier dramatically to 65 kJ/mol. It is reasonable to assume at the ZrO/ZrO_2 interface, where the oxygen activity will be low (according to an Ellingham diagram, the oxygen partial pressure in this region is very low, namely of the order of 10^{-90} atm), both phases exhibit oxygen vacancies thus facilitating the ingress of hydrogen.

Once inside oxygen-saturated Zr such as ZrO_{1-x} and Zr_3O , the present calculations show that the diffusion barriers for H are relatively low, namely in the range of 30 to 70 kJ/mol. For regions under tensile strain, as they exist near the metal/oxide interfaces, the barrier can be even lower. The thermodynamic driving forces for this H migration are (i) the free energy of solution of H in Zr metal, (ii) the precipitation of hydrides if a critical concentration of dissolved H is reached, and (iii) the associated gradients in the H concentration. Thus, once hydrogen atoms are inside the suboxide and oxygen-saturated Zr region, they will diffuse through the interface between the hexagonal ZrO into the oxygen-saturated α -Zr and onwards towards Zr metal to form dissolved H or to find nucleation sites for zirconium hydrides. This would complete the path for H from a water molecule to dissolved hydrogen or metal hydrides.

In addition, if nano-pipes larger than 1 nm in diameter exist allowing water molecules to reach suboxide, the present *ab initio* calculations show a spontaneous dissociation of water on suboxide surfaces leading to a configuration analogous to the reaction of a water molecule with an oxygen vacancy in ZrO_2 , namely the formation of an OH group and a hydridic hydrogen. After dissociation, the acidic and hydridic hydrogen atoms can react to form an H_2 molecule, which would supply additional H to dissolve in the metal or to form hydrides.

5. Discussion

Based on these new observations, and previous work on similar oxides [12, 63] we use a schematic in Figure 7(a), (b), and (c) and the quantitative pore density measurements in Figure 8 to summarize the distribution and types of porosity we observe. Most of the top part of the oxide is so porous that it can play no part in the electrochemical cell generated by the corroding metal and the aqueous environment – the porous or ‘fossil’ oxide. The electrochemical barrier, or protective, layer is only the thin region near the metal-oxide interface where no nano-pipes are observed, Figure 6(b) and (c). This barrier layer includes both suboxide and the oxygen saturated $\text{Zr}(\text{O}_{\text{sat}})$ layer with isolated pores located in the suboxide ZrO. The pore density obtained from quantitative measurements (Figure 8) increases significantly towards the oxide surface, confirming the visual impression of changes in pore concentration we gain from the images in Figure 2.

Here we should distinguish between the preferential diffusion paths for hydrogenic species offered by grain boundaries in the nano-crystalline oxide layers [8, 9, 18, 19] and the porosity described here. The nano-pores nucleate preferentially, but not exclusively, on oxide grain boundaries, and are often seen to align along grain boundary planes to form the nano-pipes, Fig. 2 a-3, b-3 and c-2. Thus although a nano-pipe is geometrically constrained to lie in an oxide grain boundary, the rapid diffusion path that they offer is not just an accelerated grain boundary diffusion phenomenon but a route by which hydrogen molecules are able to penetrate close to the metal/oxide interface.

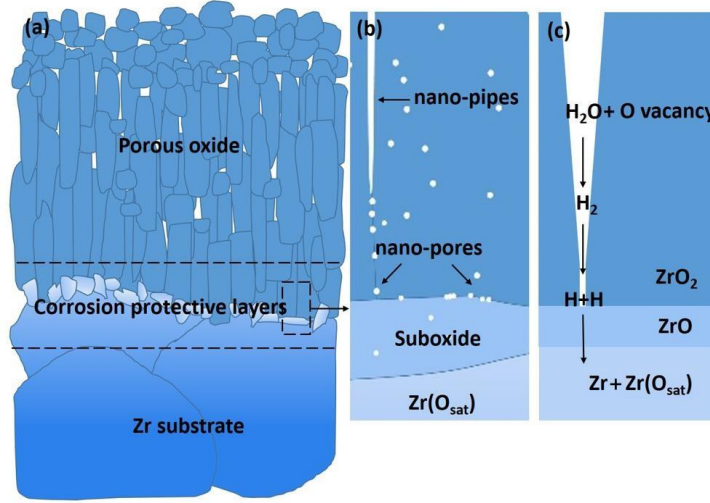


Fig. 7. Nano-pores and nano-pipes distribution in ZrO₂ corrosion films. (a) Schematic of the size and distribution of nano-pores and nano-pipes in the oxide layer. Panels (b) and (c) show magnified cartoons of nano-pores and nano-pipes in the protective oxide near the metal-oxide interface. The change in color in the metallic substrate reflects the oxygen content measured in previous work [14, 63]. The panel on the right-hand side shows the proposed mechanism for H uptake. Channels for the diffusion of molecular hydrogen can be as small as 0.5 nm and thus may not be visible in the TEM images.

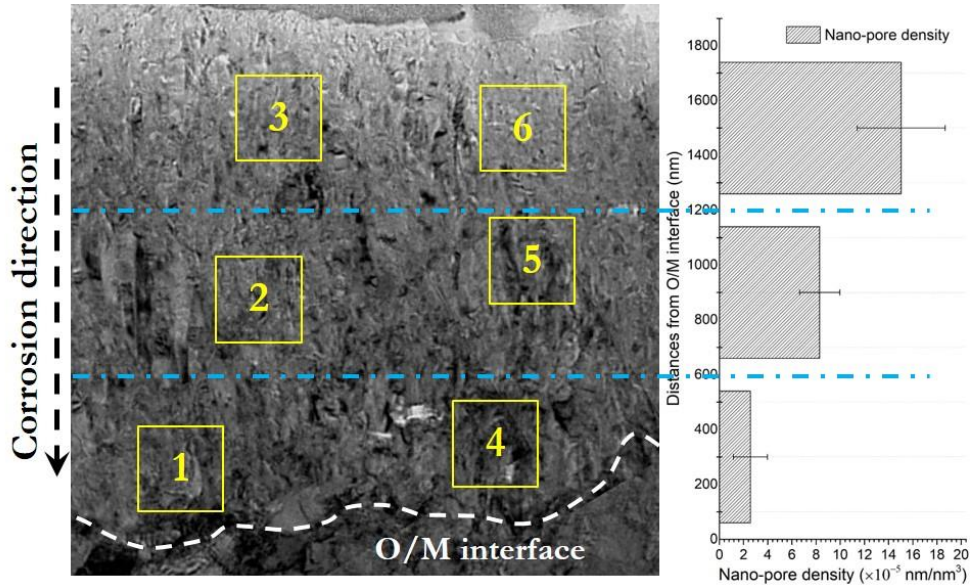


Fig. 8. Quantitative porosity measurements as a function of location in the oxide and corresponding TEM Fresnel images showing the nano-pore morphology in the oxide on the 75-day Zr-0.5% Nb sample. The inset shows regions selected for quantitative measurements. The thicknesses measured by Electron Energy Loss Spectroscopy (EELS) [64] in regions 1 and 2 are ~55nm, and in region 3 is ~35nm.

Combining these experimental observations with the results from the present simulations, we conclude that water molecules can diffuse through nano-pipes reaching a region close to the metal-oxide interface as shown in Figures 2 and 7. In this region, ZrO_2 is likely to contain a relatively high concentration of oxygen vacancies. As the present quantum mechanical calculations show, water molecules react strongly with vacancies releasing hydrogen, which recombines to form molecular H_2 . The hydrogen molecules can diffuse through nano-voids as small as 0.5 nm in diameter, *i.e.* through nano-pipes and nano-pores which are too small for the diffusion of water molecules. From these facts one must infer that molecular hydrogen is likely to be present in nanopores close to the metal-oxide interface. One possibility is the presence of a network of nano-pores with a diameter between 0.5 nm and 1 nm, which are not resolved in the present TEM images, but would allow diffusion of molecular hydrogen. Atom Probe Tomography analysis of the metal/oxide interface region of Zr-2.5Nb alloys corroded in deuterated water [65] has detected D in isolated nanopores of this size but has not observed D in nano-pipes close to the suboxide region, perhaps emphasizing the relative rarity of these penetration paths. We suggest that molecular hydrogen can easily escape during sample preparation for TEM or APT analysis, while chemically bound hydroxyl groups on the walls of nano-pipes are more likely to persist.

For the above reasons, it seems plausible that some hydrogen molecules reach the suboxide region. The present simulations demonstrate that molecular hydrogen spontaneously dissociates on suboxide (ZrO) surfaces and that ingress into these suboxide grains is energetically possible, especially for ZrO containing oxygen vacancies, thus providing a pathway for hydrogen pickup by the metal. In this mechanism, the cathodic reduction of hydrogen takes place at the sites where water molecules react with oxygen vacancies in the oxide, provided that the electronic energy level associated with the oxygen vacancy (“the vacancy level”) is occupied with electrons. As mentioned above, such neutral oxygen vacancies are likely to exist near the metal/oxide interface. The actual uptake of hydrogen from nano-pipes and nano-pores into the solid phase occurs closer to the metal/oxide interface, namely in the region of the suboxide barrier layer.

Even if no static continuous network of nano-pipes extends to the suboxide region, dynamic processes during the advance of the metal-oxide interface can temporarily open pathways for the migration of hydrogen trapped in nano-pores. In the present model, trapped hydrogen could exist in molecular form. Another possibility is the presence of H atoms occupying chains of oxygen vacancies as proposed by Lindgren *et al.* [19]. Depending on the concentration of oxygen vacancies in the region near the barrier oxide, it might then be possible for H atoms to diffuse through the oxide in a vacancy-assisted mechanism, as discussed earlier.

The present simulations show that the direct ingress of H atoms from $\text{ZrO}(0001)$ facets into defect-free ZrO is hampered by a high barrier of well over 100 kJ/mol (*cf.* Figure 6). However, the present calculations demonstrate that oxygen vacancies inside ZrO enable ingress and diffusion of H towards the metal. Such vacancies are likely to exist as the advancing front of oxidized zirconium transforms oxygen-saturated $\alpha\text{-Zr}$ of the approximate composition $\text{ZrO}_{0.3}$ into a metastable ZrO phase and subsequently into ZrO_{2-x} , which finally ends as stoichiometric ZrO_2 .

Furthermore, in the temperature range of interest, the chemical potential of an H atom inside ZrO is still lower (*i.e.* energetically more favorable) than H in the form of a molecule. In addition, ingress through a different facet of ZrO or via other oxygen-saturated phases such as Zr_3O would

provide pathways into ZrO. Once an H atom reaches the interstitial region inside ZrO, the subsequent steps towards the precipitation of a hydride involve smaller activation barriers if oxygen vacancies are present in this suboxide. Thus, the step with the highest energy barrier for the H pickup process could well be the ingress of H atoms into a suboxide after dissociative adsorption of an H₂ molecule on a suboxide surface. In fact, an experimental study of the kinetics of the reaction of an oxidized zirconium alloy with hydrogen (without water) by Une [66] suggests that the rate-controlling step of the hydrogen ingress is a phase-boundary controlled reaction with an activation energy of 68 kJ/mol. Remarkably, this value coincides with the computed barrier of 65 kJ/mol for vacancy-assisted H diffusion through the ZrO barrier layer (*cf.* Figure 6).

The other rate-limiting factors are (i) the topology of the nano-porosity of the oxide film near the metal-oxide interface, (ii) the concentration and accessibility of oxygen vacancies in this region, and (iii) the charge neutrality of these oxygen vacancies.

Given these rate-limiting factors, one could rationalize the effect of alloying Zr with Nb which empirically is known to reduce the hydrogen pickup fraction [67-69]. Comparing Figure 2(a) and (c), one can see that the oxide films in both of the Zr-Nb samples, Figure 2(a) and (b) have a lower concentration of nano-porosity than the oxide on Zircaloy-4, Figure 2(c), which would correlate directly with the measured lower hydrogen pick up fraction because fewer H atoms could reach the metal-oxide boundary.

There may well be other mechanisms enabling the transport of hydrogen through oxide films. For example, a recent computational work by Sato *et al.* using *ab initio* molecular dynamics [6] demonstrated the hopping of protons on a hydrated surface of cubic ZrO₂. This mechanism is likely to occur if (i) the pH of the aqueous phase is low, *i.e.* if the surface is acidic and there are enough protons in solution, and (ii) the oxide surface inside cracks or pores is in contact with water. However, this transport mechanism does not address the cathodic reaction that would be necessary to reduce a solvated H₃O⁺ ion into a negatively charged hydridic H atom migrating into the suboxide and ultimately into Zr metal to form hydrides. The same issue exists with mechanisms involving hydrogen transport as H⁺ through the oxide via a vacancy-assisted mechanism. In this model it remains unclear, at which site the reduction from a proton to a hydridic hydrogen would take place. It could occur inside the oxide in regions with a sufficiently high local Fermi level or at phase boundaries.

In the present model, the reduction of the H atoms of the water molecules to neutral H atoms would occur directly at the site where a water molecule fills a neutral surface vacancy and an H₂ molecule is formed. Here, a “neutral vacancy” means an oxygen vacancy with occupied electronic levels originating from the dangling bonds of the neighboring Zr atoms.

This would be the cathodic site deep inside the oxide layer. In the case of doping with niobium, the excess electrons from the Nb atoms would provide the electrons to neutralize oxygen vacancies in regions closer to the oxide/water interface, thus moving the reduction site away from the metal-oxide interface and thereby reducing the hydrogen pickup fraction, as seen in experiments.

6. Summary and Conclusion

In summary, the present combined experimental and computational investigation provides evidence for a possible mechanism of hydrogen pickup resulting from the oxidation of a metal by water. In this proposed mechanism, water molecules penetrate through cracks of the outer porous layers of the corrosion film into regions of significant concentrations of oxygen vacancies. Water molecules fill vacancies in a highly exothermic reaction with H atoms dissociating and forming spontaneously molecular hydrogen. These H₂ molecules escape either to the oxide/water interface and dissolve in the aqueous phase or they diffuse through cracks and nano-pipes through the porous oxide reaching the layer of suboxides near the metal/oxide interface. Hydrogen molecules dissociate spontaneously on suboxides such as ZrO. The newly formed H atoms penetrate into the suboxide, diffuse further through regions of oxygen saturated zirconium metal towards the interior of the unoxidized metal, finally forming thermodynamically stable zirconium hydrides that act as sink for hydrogen atoms. The present work shows that (i) pathways for this process are likely to exist in the form of nano-pipes and (ii) the uptake of H atoms into suboxides forms the highest energy barrier of approximately 65 kJ/mol. Thus, a possible mechanism leading to hydrogen pickup during the oxidation of zirconium in an aqueous environment has been identified.

While the oxidation of zirconium and its alloys exhibit unique features, it is reasonable to assume that the mechanism described in the present work occurs also in the oxidation of other metals and alloys with nano-porous oxide films. In any case, a key experiment to help refine our understanding would be the detection of molecular hydrogen inside oxide films close to the metal-oxide interface, either as a diffusing species in nano-pipes or trapped in nano-pores.

In conclusion, the present work demonstrates the power of combining high-resolution experimental characterization with computational materials modeling and simulations in unravelling complex processes such as the oxidation and hydrogen pickup of metals exposed to aqueous environments.

Acknowledgements

This project is part of the MUZIC-2 (Mechanistic Understanding of Zirconium Corrosion and Hydrogen Pickup-2) and EPRI SHIZAM (Study of Hydrogen Impacts in Zirconium Alloy Materials) collaboration. The contributions by the members of the EPRI SHIZAM and the MUZIC programs were critical for the present work and are very much appreciated. The authors gratefully acknowledge support from Westinghouse and EPRI, and many useful discussions within the consortium. Jing Hu is supported by the China Scholarship Council. EPSRC grants (EP/K040375/1 and EP/N010868/1) are acknowledged for funding the ‘South of England Analytical Electron Microscope’ and the Zeiss Crossbeam FIB/SEM used in this research.

References

- [1] H.G. Rickover, L.D. Geiger, B. Lustman, History of the development of zirconium alloys for use in nuclear reactors. (TID-26740), Energy Research and Development Administration, Washington, D.C. (USA). Div. of Naval Reactors (1975).
- [2] C.E. Coleman, D. Hardie, The hydrogen embrittlement of α -zirconium—A review. *J. Less Common Met.* 11 (1966) 168–185.
- [3] E. Hillner, Hydrogen absorption in zircaloy during aqueous corrosion: effect of environment, Washington, D.C.: Office of Technical Services, Department of Commerce (1964).
- [4] T. Smith, Kinetics and mechanism of hydrogen permeation of oxide films on zirconium. *J. Nucl. Mater.* 18 (1966) 323–336.
- [5] B. Malki, O. Le Bacq, A. Pasturel, *Ab initio* study of hydrogen related defect in ZrO_2 : Consequences on dry and aqueous oxidation, *J. Nucl. Mater.* 416 (2011) 362–368.
- [6] R. Sato, S. Ohkuma, Y. Shibuta, F. Shimojo, S. Yamaguchi, Proton Migration on Hydrated Surface of Cubic ZrO_2 : *Ab initio* Molecular Dynamics Simulation, *J. Phys. Chem. C* 119 (2015) 28925–28933.
- [7] R.B.L. Vieira, R.C. Vilão, A.G. Marinopoulos, P.M. Gordo, J.A. Paixão, H.V. Alberto, J.M. Gil, A. Weidinger, R.L. Lichti, B. Baker, P.W. Mengyan, J.S. Lord, Isolated hydrogen configurations in zirconia as seen by muon spin spectroscopy and *ab initio* calculations, *Phys. Rev. B* 94 (2016) 115207.
- [8] B. Cox, Y.-M. Wong, A hydrogen uptake micro-mechanism for Zr alloys, *J. Nucl. Mater.* 270 (1999) 134–146.
- [9] M. Lindgren, G. Sundell, I. Panas, L. Hallstadius, M. Thuvander, H-O. Andrén, in *Zirconium in the Nuclear Industry: 17th Vol.* 515–539 (ASTM International, 2015). doi:10.1520/STP154320120164.
- [10] X. Iltis, H. Michel, Transmission Electron Microscopy Study of a Locally Ordered Zr-O Solid-Solution Obtained by an Oxidation Treatment of a Zircaloy-4 Alloy, *J. Alloys Compd.* 177 (1991) 71–82.
- [11] P. Tejlund, M. Thuvander, H.-O. Andrén, S. Ciurea, T. Andersson, M. Dahlbäck, L. Hallstadius, Detailed Analysis of the Microstructure of the Metal/Oxide Interface Region in Zircaloy-2 after Autoclave Corrosion Testing, *J. ASTM Int.*, 8 (2011), Paper ID JAI102956.
- [12] N. Ni, D. Hudson, J. Wei, P. Wang, S. Lozano-Perez, G.D.W. Smith, J.M. Sykes, S.S. Yardley, K.L. Moore, S. Lyon, R. Cottis, M. Preuss, C.R.M. Grovenor, How the crystallography and nanoscale chemistry of the metal/oxide interface develops during the aqueous oxidation of zirconium cladding alloys, *Acta Mater.* 60 (2012) 7132–7149.
- [13] B. de Gabory, Y. Dong, A.T. Motta, E.A. Marquis, EELS and atom probe tomography study of the evolution of the metal/oxide interface during zirconium alloy oxidation, *J. Nucl. Mater.* 462 (2015) 304–309.
- [14] J. Hu, B. Setiadinata, T. Aarholt, A. Garner, A. Vilalta-Clemente, J.M. Partezana, P. Frankel, P. Bagot, S. Lozano-Perez, A. Wilkinson, M. Preuss, M. Moody, C.R.M. Grovenor, Understanding Corrosion and Hydrogen Pickup of Zirconium Fuel Cladding Alloys: The Role of Oxide Microstructure, Porosity, Suboxides, and Second-Phase Particles, *Zirconium in the Industry: 18th International Symposium* (2018), doi:10.1520/STP159720160071.
- [15] J. Hu, A. Garner, N. Ni, A. Gholinia, R.J. Nicholls, S. Lozano-Perez, P. Frankel, M. Preuss, C.R.M. Grovenor, Identifying suboxide grains at the metal-oxide interface of a corroded Zr-1.0%Nb alloy using (S)TEM, transmission-EBSD and EELS, *Micron* 69 (2015) 35–42.

- [16] N. Ni, S. Lozano-Perez, M.L. Jenkins, C. English, G.D.W. Smith, J.M. Sykes, C.R.M. Grovenor, Porosity in oxides on zirconium fuel cladding alloys, and its importance in controlling oxidation rates, *Scr. Mater.* 62 (2010) 564–567.
- [17] J. Heikinheimo, S. Ortner, I. Makkonen, J. Kujala, M. Blackmur and F. Tuomisto, Positron annihilation analysis of the atomic scale changes in oxidized Zircaloy-4 samples, *J. Nucl. Mater.* 495 (2017) 172–180.
- [18] M. Lindgren, I. Panas, Impact of Additives on Zirconium Oxidation by Water: Mechanistic Insights from First Principles, *RSC Advances* 3 (2013) 21613–21619.
- [19] M. Lindgren, C. Geers, I. Panas, Possible origin and roles of nano-porosity in ZrO_2 scales for hydrogen pick-up in Zr alloys", *J. Nucl. Mater.* 492 (2017) 22–31.
- [20] B. Cox, A mechanism for the hydrogen uptake process in zirconium alloys, *J. Nucl. Mater.* 264 (1999) 283–294.
- [21] A. Couet, A.T. Motta, R.J. Comstock, Hydrogen pickup measurements in zirconium alloys: Relation to oxidation kinetics, *J. Nucl. Mater.* 451 (2014) 1–13.
- [22] S. Lozano-Perez, A guide on FIB preparation of samples containing stress corrosion crack tips for TEM and atom-probe analysis, *Micron* 39 (2008) 320–328.
- [23] M. Ruehle, M. Wilkens, Defocusing contrast of cavities, *Cryst. Lattice Defects* 6 (1975) 129–140.
- [24] N. Ni, Study of Oxidation Mechanisms of Zirconium Alloys by Electron Microscopy, Univ. Oxford PhD Thesis (2011).
- [25] K. Iakoubovskii, K. Mitsuishi, Y. Nakayama, K. Furuya, Thickness measurements with electron energy loss spectroscopy. *Microsc. Res. Tech.* 71 (2008) 626–631.
- [26] P. Hohenberg, W. Kohn, Inhomogenous Electron Gas, *Phys. Rev.* 136 B (1964) 864–871.
- [27] W. Kohn, L.J. Sham, Self-Consistent Equations Including Exchange and Correlation Effects, *Phys. Rev.* 140 A (1965) 1133–1138.
- [28] J.P. Perdew, K. Burke, M. Ernzerhof, Generalized Gradient Approximation Made Simple, *Phys. Rev. Lett.* 77 (1996) 3865–3868.
- [29] P.E. Blöchl, Projector augmented-wave method, *Phys. Rev. B* 50 (1994) 17953–17979.
- [30] G. Kresse, J. Hafner, Ab Initio Molecular Dynamics of Liquid Metals, *Phys. Rev. B* 47 (1993) 558–561.
- [31] G. Kresse, J. Furthmüller, Efficient iterative schemes for ab initio total-energy calculations using a plane-wave basis set, *Phys. Rev. B* 54 (1996) 11169–11186.
- [32] MedeA: Materials Exploration and Design Analysis, Materials Design, Inc., San Diego, CA, U.S.A. (2018).
- [33] G. Henkelman, B.P. Uberuaga, H. Jónsson, A climbing image nudged elastic band method for finding saddle points and minimum energy paths, *J. Chem. Phys.* 113 (2000) 9901–9904.
- [34] H. Sun, S.J. Mumby, J.R. Maple, A.T. Hagler, An ab Initio CFF93 All-Atom Force Field for Polycarbonates, *J. Am. Chem. Soc.* 116 (1994) 2978–2987.
- [35] M. Waldman, A.T. Hagler, New combining rules for rare gas van der waals parameters. *J. Comput. Chem.* 14 (1993) 1077–1084.
- [36] S. Plimpton, Fast Parallel Algorithms for Short-Range Molecular Dynamics, *J. Comput. Phys.* 117 (1995) 1–19.
- [37] A. Yilmazbayhan, A.T. Motta, R.J. Comstock, G.P. Sabol, B. Lai, Z. Cai, Structure of zirconium alloy oxides formed in pure water studied with synchrotron radiation and optical microscopy: relation to corrosion rate, *J. Nucl. Mater.* 324 (2004) 6–22.

- [38] A.T. Motta, J. Bischoff, A. Siwy, M.J. Gomes da Silva, R.J. Comstock, Z. Cai, B. Lai, Characterization of Oxide Layers Formed During Corrosion in Supercritical Water, Paper No. 4868, 17th International Corrosion Congress, NACE International (2008).
- [39] A. Yilmazbayhan, E. Breval, A.T. Motta, R.J. Comstock, Transmission electron microscopy examination of oxide layers formed on Zr alloys, *J. Nucl. Mater.* 349 (2006) 265–281.
- [40] B. Cox, Mechanisms of Hydrogen Absorption by Zirconium Alloys (AECL--8702), Atomic Energy of Canada Limited, Chalk River, Ontario, Canada (1985).
- [41] A. Yilmazbayhan, A.R. Motta, R.J. Comstock, G.P. Sabol, B. Lai, Z. Cai, Structure of zirconium alloy oxides formed in pure water studied with synchrotron radiation and optical microscopy: Relation to corrosion rate, *J. Nucl. Mater.* 324 (2004) 6–22.
- [42] P. Bossis, G. Lelièvre, P. Barberis, X. Iltis, F. Lefebvre, Multi-Scale Characterization of the MetalOxide Interface of Zirconium Alloys, in *Zirconium in the Nuclear Industry: Twelfth International Symposium* 918-918–27 (ASTM International, 2000), doi:10.1520/STP14334S.
- [43] V.N. Shishov, M.M. Peregud, A.V. Nikulina, V.F. Kon'kov, V.V. Novikov, V.A. Markelov, T.N. Khokhunova, G.P. Kobylansky, A.E. Novoselov, Z.E. Ostrovsky, A.V. Obukhov, Structure-Phase State, Corrosion and Irradiation Properties of Zr-Nb-Fe-Sn System Alloys. *J. ASTM Int.* 5 (2008) 724–743.
- [44] H.G. Kim, S.Y. Park, M.H. Lee, Y.H. Jeong, S.D. Kim, Corrosion and microstructural characteristics of Zr–Nb alloys with different Nb contents. *J. Nucl. Mater.* 373 (2008) 429–432.
- [45] B. de Gabory, A.T. Motta, K. Wang, Transmission electron microscopy characterization of Zircaloy4 and ZIRLO oxide layers. *J. Nucl. Mater.* 456 (2015) 272–280.
- [46] H. Göhr, J. Schaller, H. Ruhmann, F. Garzarolli, Long-Term In Situ Corrosion Investigation of Zr Alloys in Simulated PWR Environment by Electrochemical Measurements, in *Zirconium in the Nuclear Industry: Eleventh International Symposium* 181-181–22 (ASTM International, 1996), doi:10.1520/STP16173S.
- [47] P. Barberis, A. Frichet, Characterization of Zircaloy-4 oxide layers by impedance spectroscopy, *J. Nucl. Mater.* 273 (1999) 182–191.
- [48] H. Beie, A. Mitwalsky, F. Garzarolli, H. Ruhmann, H. Sell, Examinations of the Corrosion Mechanisms of Zirconium Alloys, in *Zirconium in the Nuclear Industry: Tenth International Symposium* 615-615–29 (ASTM International, 1994), doi:10.1520/STP15212S.
- [49] A. Kumar, M. Nasrallah, D.L. Douglass, The effect of yttrium and thorium on the oxidation behavior of Ni-Cr-Al alloys, *Oxid. Met.* 8 (1974) 227–263.
- [50] Kammenzind, B.F., Eklund, K.L., and Bajaj, R., The Influence of In-Situ Straining on the Corrosion of Zircaloy in a PWR Water Environment, Thirteenth International Symposium on Zirconium in the Nuclear Industry, ASTM-STP 1423, 2002.
- [51] J. Romero, J. Partezana, R.J. Comstock, L. Hallstadius, Evolution of Hydrogen Pickup Fraction with Oxidation Rate on Zirconium Alloys. *TopFuel* (2015) 1–7.
- [52] A.T. Motta, M.J. Gomes da Silva, A. Yilmazbayhan, R.J. Comstock, Z. Cai, B. Lai, Microstructural Characterization of Oxides Formed on Model Zr Alloys Using Synchrotron Radiation. *J. ASTM Int.* 5 (2008) 101257.
- [53] P. Lazar, M. Otyepka, Dissociation of Water at Iron Surfaces: Generalized Gradient Functional and Range-Separated Hybrid Functional Study, *J. Phys. Chem. C* 116 (2012) 25470–25477.
- [54] Y. Kim, R. Lynden-Bell, A. Alavi, J. Stulz, D. Goodman, Evidence for partial dissociation of water on flat MgO(100) surfaces, *Chem. Phys. Lett.* 352 (2002) 318–322.

- [55] R. Lynden-Bell, L. Delle Site, A. Alavi, Structures of adsorbed water layers on MgO: an ab initio study, *Surf. Sci.* 496 (2002) L1–L6.
- [56] B. Cox, Some thoughts on the mechanisms of in-reactor corrosion of zirconium alloys, *J. Nucl. Mater.* 336 (2005) 331–368.
- [57] R.F.W. Bader, A Quantum Theory of Molecular Structure and Its Applications, *Chem. Rev.* 91 (1991) 893–928.
- [58] A. Garner, A. Gholinia, P. Frankel, M. Gass, I. MacLaren, M. Preuss, The microstructure and microtexture of zirconium oxide films studied by transmission electron backscatter diffraction and automated crystal orientation mapping with transmission electron microscopy. *Acta Mater.* 80 (2014) 159–171.
- [59] D.J. Spengler, A.T. Motta, R. Bajaj, J.R. Seidensticker, Z. Cai, Characterization of Zircaloy-4 corrosion films using microbeam synchrotron radiation, *J. Nucl. Mater.* 464 (2015) 107–118.
- [60] A. Garner, M. Preuss, P. Frankel, A method for accurate texture determination of thin oxide films by glancing-angle laboratory X-ray diffraction. *J. Appl. Cryst.* 47 (2014) 575–583.
- [61] Materials Modeling of Hydrogen Pickup in Zirconium Alloys. EPRI, Palo Alto, CA (2017) 3002009576.
- [62] N. Ni, D. Hudson, J. Wei, P. Wang, S. Lozano-Perez, G.D.W. Smith, J.M. Sykes, S.S. Yardley, K.L. Moore, S. Lyon, R. Cottis, M. Preuss, C.R.M. Grovenor, How the crystallography and nanoscale chemistry of the metal/oxide interface develops during the aqueous oxidation of zirconium cladding alloys. *Acta Mater.* 60 (2012) 7132–7149.
- [63] J. Hu, R. Nicholls, S. Lozano-Perez, C.R.M. Grovenor, A. Garner, A. Gholinia, P. Frankel, M. Preuss, N. Ni, High-resolution characterization of corrosion and hydrogen pickup of Zr cladding alloys, China Nuclear Energy Association, TopFuel (2015).
- [64] T. Malis, S.C. Cheng, R.F. Egerton, EELS log-ratio technique for specimen-thickness measurement in the TEM, *J. Electron Microsc. Tech.* 8 (1988) 193–200.
- [65] G. Sundell, M. Thuvander, A.K. Yatim, H. Nordin, H.-O. Andrén, Direct observation of hydrogen and deuterium in oxide grain boundaries in corroded Zirconium alloys, *Corros. Sci.* 90 (2015) 1–4.
- [66] K. Une, Kinetics of reaction of zirconium alloy with hydrogen, *J. Less Common Met.* 57 (1978) 93–101.
- [67] A. Couet, A.T. Motta, R.J. Comstock, Effect of Alloying Elements on Hydrogen Pickup in Zirconium Alloys, ASTM International STP1543 (2014) 479–509.
- [68] M. Youssef, M. Yang, B. Yildiz, Doping in the Valley of Hydrogen Solubility: A Route to Designing Hydrogen-Resistant Zirconium Alloys, *Phys. Rev. Appl.* 5 (2016) 014008.
- [69] B.D.C. Bell, S.T. Murphy, R.W. Grimes, M.R. Wenman, The effect of Nb on the corrosion and hydrogen pick-up of Zr alloys, *Acta Mater.* 132 (2017) 425–431.